

An improved mathematical model and finite-element study of dynamically coupled metal-hydride reactors – Part 1: Model development

Author

Parida, A, Gray, EMA, Muthukumar, P, Dalal, A

Published

2025

Journal Title

International Journal of Hydrogen Energy

Version

Version of Record (VoR)

DOI

[10.1016/j.ijhydene.2025.150692](https://doi.org/10.1016/j.ijhydene.2025.150692)

Rights statement

© 2025 The Authors. Published by Elsevier Ltd on behalf of Hydrogen Energy Publications LLC. This is an open access article under the CC BY license (<http://creativecommons.org/licenses/by/4.0/>).

Downloaded from

<https://hdl.handle.net/10072/438858>

Griffith Research Online

<https://research-repository.griffith.edu.au>



An improved mathematical model and finite-element study of dynamically coupled metal-hydride reactors – Part 1: Model development

Abhishek Parida ^{a,b}, Evan MacA. Gray ^{a,*}, P. Muthukumar ^c, Amaresh Dalal ^b

^a Queensland Micro- and Nanotechnology Centre, Griffith University, Nathan, 4111, Australia

^b Department of Mechanical Engineering, Indian Institute of Technology Guwahati, Guwahati, Assam, 781039, India

^c Department of Mechanical Engineering, Indian Institute of Technology Tirupati, Tirupati, Andhra Pradesh, 517619, India

ARTICLE INFO

Handling Editor: Dr. E.A. Veziroglu

Keywords:

Metal hydride
Compressor
Heat pump
Coupled model
Finite-element

ABSTRACT

Many modelling studies have been conducted on single metal-hydride (MH) beds subject to, for example, a sudden increase in hydrogen pressure. In a practical MH thermodynamic machine such as a hydrogen compressor or heat pump, however, one bed is heated and desorbs into a second, cooled bed. This two-part study presents a two-dimensional axisymmetric mathematical model for such thermodynamic machines, simulating two interconnected cylindrical MH tanks, constrained so that the mass flow rate from the desorbing bed equals the inlet flow rate of the absorbing bed. Part 1 covers the development of the model and its validation against experiment. Key practical MH characteristics like expansion, hysteresis and plateau slope are accounted for. Implemented using COMSOL Multiphysics, the model simulates horizontal annular reactors containing different AB₅ alloys, with finned coaxial heat exchangers. This configuration was chosen to expose the existence and consequences of internal temperature gradients arising in the low effective thermal conductivity of MH beds. The model incorporates mathematical formulations to account for variations in bed porosity and permeability arising from changes in alloy particle diameter during volumetric expansion and contraction induced by hydrogen absorption and desorption. These variations influence the effective thermal conductivity within the bed, which is also captured by the model. In Part 2 the model is utilised to investigate the underlying physics governing coupled-reactor operation, with its advantages over conventional single-reactor models comprehensively analysed.

Nomenclature

B	Shape factor
b	Dimensionless constant
c	Specific heat (kJ/(kg × K))
C	Reaction constant (1/s)
d	Diameter (m)
E	Activation energy (J/mol)
H	Enthalpy (J/mol)
k	Thermal conductivity (W/(m × K))
K	Boltzmann constant (J/K)
l	Length of reactor (m)
m	Volumetric rate of mass transferred by MH (kg/(m ³ × s))
m	Mass (kg)
M	Molecular weight (kg/mol)
n	Normal vector
N	Number of hydrogen atoms
p	Bed pressure (Pa)
P	External or equilibrium pressure (Pa)

(continued on next column)

(continued)

Q	Heat (J)
r	Radius (m)
S	Entropy (J/K)
R	Universal gas constant (J/(kg × K))
t	Time (s) and fin thickness (mm)
T	Temperature (K)
v	Superficial velocity (m/s)
V	Volume of hydrogen transferred (L)
$w\%$	Weight percentage
X	Reacted fraction
Z	Compressibility factor

Greek letters

α	α phase
β	β phase
ϵ	Bed porosity
κ	Permeability (m ²)
λ	Mean free path (m)
μ	Dynamic viscosity (Pa.s)

(continued on next page)

* Corresponding author.

E-mail address: e.gray@griffith.edu.au (E.MacA. Gray).

<https://doi.org/10.1016/j.ijhydene.2025.150692>

Received 27 January 2025; Received in revised form 9 July 2025; Accepted 25 July 2025

Available online 22 August 2025

0360-3199/© 2025 The Authors. Published by Elsevier Ltd on behalf of Hydrogen Energy Publications LLC. This is an open access article under the CC BY license (<http://creativecommons.org/licenses/by/4.0/>).

(continued)

ρ	Density (kg/m ³)
γ	Hysteresis
σ	stress tensor (N/m ²)
δ	Strain tensor
Ψ	Concentration
φ_s, φ_o	Slope factor
ω	Specific internal energy (J/kg)
ξ	Volume expansion factor
Acronyms	
CR	Critical
MH	Metal hydride
HTF	Heat transfer fluid
PCT	Pressure composition temperature
Subscripts	
a	Absorption
$alloy$	Metal hydride alloy
d	Desorption
ed	Empty
e	Effective
eq	Equilibrium
f	fluid
F	Fin
g	Gas
H_2	Hydrogen gas
i	Initial
$inlet$	Inlet boundary
MH	Metal hydride
o	Empty/outer
p	Particle
r	Radial distance
rad	Radiation

1. Introduction

Metal-hydride-based hydrogen systems are attracting significant global research attention as key enablers of sustainable energy solutions, including hydrogen storage, compression, and space heating/cooling. Their ability to reversibly absorb and desorb hydrogen under controlled conditions makes them integral to renewable energy-driven hydrogen supply chains [1]. Large-scale experimental studies are often limited by cost and resource constraints, highlighting the critical role of mathematical models. These models bridge the gap by elucidating the complex thermal, mass, and momentum transfer phenomena in metal-hydride (MH) systems, facilitating physics-based insights and system optimisation for real-world applications [2].

Interstitial metal hydrides, in which dissociated H species occupy interstices in the metal crystal, are attractive for hydrogen storage because of their capacity for high-density storage and enhanced safety features. Metal hydrides more generally encompass single metal elements, metallic alloys and intermetallic compounds that reversibly react with hydrogen to form hydrides, and complex hydrides that are much more difficult to use. Interstitial MHs formed from alloys and intermetallic compounds are particularly attractive for applications because of the tunability of their thermodynamic and operating characteristics by changing the proportions of the constituent elements. The uptake of atomic hydrogen by the metal is exothermic and its release is endothermic. The thermodynamic and operating characteristics of MHs are linked by the (approximate) van 't Hoff relation:

$$\ln(p_a / p_0) = \frac{1}{R} \left(\frac{\Delta H}{T} - \Delta S \right) \quad (1)$$

for the reaction in which a dilute solid-solution phase (α) transforms to a concentrated hydride phase (β) at notionally constant pressure p_a . Here ΔH and ΔS are respectively the enthalpy and entropy change per mole H_2 associated with the hydriding reaction, referred to pressure p_0 . Both are negative. Desorption occurs at a lower pressure, with slightly different values of $|\Delta H|$ and $|\Delta S|$, therefore. The textbook by Fukai provides an extensive introduction to metal- H_2 systems [1].

While hydrogen storage is the most-often discussed application of

MHs, other applications exist [3]. In the context of the present paper, the relationship between pressure and temperature established by the values of ΔH and ΔS supplies the basis for building thermodynamic machines with hydrogen working gas: a metal charged with hydrogen at low pressure and temperature releases hydrogen at a higher pressure when heated. Two MH beds with suitable thermodynamic characteristics may be coupled to make a two-stage compressor or a heat pump. Utilisation of MHs in hydrogen compressors and heat pumps respectively was reviewed by Lotosky et al. [4] and Muthukumar et al. [5].

Coupling one or more pairs of MH beds to build a thermodynamic machine has two important aspects. First, thermodynamic matching of the paired hydrogen storage alloys is needed to ensure that the desorbing bed empties into the absorbing bed (and vice versa) under the intended conditions of pressure and temperature. This aspect was considered in detail for heat pumps by Dantzer and Orgaz [6] and for compressors by Gray [7] and Cousins et al. [8]. In this approach, alloy pairs are typically selected based on suitable combinations of enthalpy and entropy changes that enable operation between the desired supply and delivery pressures using Eqn. (1). While this method effectively determines the compression ratio for a multistage MH compressor and helps narrow down potential alloy pairs, it does not provide insight into the quantity or duration of hydrogen transfer. Second, dynamic matching of the two MH beds is needed to ensure that the rate of desorption by one bed is matched by the rate of absorption of the second bed. This aspect has received relatively little attention in the literature.

The enthalpy of reaction for MHs that could be considered for building thermodynamic machines typically ranges from about 17 to about 52 kJ/mol. H_2 [4], making thermal management critical in such MH systems. Given that metal hydrides are stored as powders in metal tanks, with hydrogen occupying the voids, the rate of chemical reaction and the resulting thermal energy generated or consumed varies with operating conditions influencing the mass transfer rate. Consequently, the overall process is governed by complex interdependencies among thermodynamics, mass transfer and chemical kinetics within the porous alloy bed, governed by variables such as temperature, pressure, fluid velocity, and hydrogen concentration varying with time. The intricacy of these interactions necessitates a mathematical model for MH systems that can provide crucial insights into operational parameters and significantly reduce expenditure on prototypes. Hence, great efforts were made to develop computationally effective mathematical models during the last several decades.

Preliminary research on MH systems dates back to the 1970s [9–11], with the first notable advancement in mathematical modelling emerging in the 1980s, when Osery [12] developed a foundational one-dimensional model. This model focused exclusively on cylindrical bed geometries and incorporated several simplifying assumptions, such as considering temperature variation to be solely radial and neglecting the influence of hydrogen flow. The model was a basic conductive framework, solved through a non-dimensional approach using a finite-difference method. Similarly, Lucas and Richards [13] developed a one-dimensional mathematical model to examine radial temperature variations in a magnesium-hydride bed enclosed in an aluminium shell, incorporating the effects of hydrogen flow. However, the predicted reaction rates exhibited significant deviations from experimental measurements, indicating the limitations of the model in accurately capturing the intricate dynamics of hydrogen-metal interactions and heat transfer processes within the porous MH bed. Sun and Deng [14] developed a more advanced model by considering the coupled heat and mass transfer in two dimensions. However, the model excluded the inertial term in the energy conservation equation, effectively neglecting the influence of hydrogen flow dynamics within the porous bed. Additionally, the model assumed boundary conditions such as constant temperature and heat flux, which are often unrealistic under actual operating conditions, thereby limiting its applicability to real-world scenarios.

Aside from model development, one of the most important

fundamental contributions was the recognition that the kinetics of hydrogen uptake in a powdered bed is dominated by heat flow rather than the intrinsic rate kinetics of the metal–hydrogen reaction, because the effective thermal conductivity is much lower than that of the metal itself [15,16].

Jemni and Nasrallah [17–19] explored various two-dimensional mathematical models for a cylindrical MH reactor containing LaNi₅ during absorption and desorption. These models made significant advances toward generalising solutions across different geometries and analytical challenges related to MH systems. Notably, the hydrogen momentum equation was addressed using Darcy's Law, and the models considered the non-thermodynamic equilibrium between the solid bed and the entrapped hydrogen gas. Sensitivity analyses were conducted on key parameters, including reactor geometry, inlet and outlet pressure, heat-transfer fluid temperature, and thermal conductivity, to evaluate their impact on the thermal response of the bed. The studies revealed that the assumption of one-dimensional heat transfer is only applicable at extreme h/R ratios (either very low or very high) where h represents reactor height and R is reactor radius. For intermediate aspect ratios, two-dimensional effects become significant and should not be ignored. However, these models had several limitations: they neglected bed expansion and contraction, assumed constant thermal conductivity and permeability, and relied on a constant-heat-flux boundary condition during the sorption process. Despite these drawbacks, these foundational studies paved the way for more advanced models, establishing a critical baseline for future research in MH reactor modelling.

During the 2000s, researchers increasingly focused on utilising mathematical models to design MH reactors with various geometries, aiming to develop thermally effective systems. Mellouli et al. [20,21] demonstrated the mathematical modelling of MH storage tanks by comparing configurations with finned and un-finned spiral tube heat exchangers. Their model, solved using the finite-volume method, was based on the control domain concept previously introduced by Jemni and Nasrallah [17]. The primary focus was on optimising charging and discharging times by analysing the influence of geometric parameters. However, the model did not account for volume expansion within the alloy bed or the dynamic effects of heat-transfer-fluid flow, relying instead on an empirical formula for a constant heat transfer coefficient at the solid–fluid interface. Similarly, Muthukumar et al. [22–24] developed both two-dimensional and three-dimensional models using COMSOL Multiphysics to study reactors ranging from prototype to industrial scale. These models also neglected the effects of volume change in the alloy bed. However, the study incorporated a unique expression for equilibrium pressure, developed by Nishizaki et al. [25], which accounted for the inherent bed hysteresis and sloping plateau characteristics of the alloy, factors that had been previously overlooked. The study primarily examined the impact of increasing the number of embedded coolant tubes within the porous bed, in addition to varying operating parameters such as supply pressure and heating and cooling fluid temperature. Despite these advances, the omission of volume-change effects remains a critical gap in accurately modelling the thermal and mass-transfer dynamics in MH systems. Meanwhile, the models developed by Hardy and Anton [26,27] bypassed the impact of hysteresis and concentration variation on the equilibrium pressure by relying on the ideal van't Hoff equation (Eqn (1)). Such models, despite their simplifications, are valuable tools for analysing various reactor geometries and fin configurations. Subsequent studies [28–31] have employed these models to evaluate and identify optimal geometrical configurations.

However, when assessing the effectiveness of MH reactors in real-world applications such as charging from an electrolyser or supplying a fuel cell (FC) at a constant rate, these models often fall short in providing accurate predictions. This discrepancy arises primarily from the boundary conditions assumed at the hydrogen inlet and outlet. Most models assume constant injection and discharge pressures, whereas real systems typically operate under flow control. This represents a

significant research gap that has been addressed by only a limited number of studies. Raju et al. [32] developed a zeroth-order (only temporal) model to examine the refuelling dynamics of a MH tank during fuel cell operation. Mohammadshahi et al. [33,34] went further by creating a two-dimensional computational model using COMSOL Multiphysics. This model accounted for flow-rate-controlled filling, simulating electrolyser injection by a Heaviside function, and discharging at a set flow rate unlike prior models that assumed constant pressure desorption. The study also incorporated volume changes during reactions. The authors [35] have also demonstrated a three-dimensional mathematical model to simulate the coupling between a MH reactor equipped with multiple coolant tubes with that of a fuel cell. Further references can be found in the review by Mohammadshahi et al. [2], with some newer references in the paper by Arslan et al. [36].

Practical thermal machines employing metal hydrides, such as compressors, thermal energy storage systems, heat pumps and refrigeration units operate using pairs of interconnected reactor beds for hydrogen exchange. The dynamics of hydrogen transport in these systems extends beyond the thermal and chemical behaviour of individual reactors, relying on the coupled interaction between pairs of reactors. Despite numerous advances, current mathematical models still fail to capture fully the complexities of the processes involved in hydrogen transport and thermal management in coupled MH systems. For instance, d'Entremont et al. [37] developed a 2-D hydrogen transport model to simulate a high-temperature thermal energy storage module using Mg₂Fe and Na₃Al, operating at 400–450 °C. Although this model aimed to assess the technical feasibility of such coupling, it overlooked critical factors like hysteresis and plateau slope, which significantly influence the coupling process [7]. Mallewarao et al. [38] made efforts to improve upon these shortcomings, yet their 2-D model still neglected volume change and assumed constant permeability when simulating dynamically coupled thermal energy storage systems. Similarly, Minko et al. [39] studied a dual-stage MH hydrogen compressor using simplified one-dimensional mass and energy balance equations that disregarded volume change. The dual-stage compressor model by Gkanas et al. [40] adopted a constant heat flux boundary condition to simplify the conjugative heat transfer problem. Some of the other similar studies are [41,42].

Some efforts to quantify the effects of volume change in MH systems have only emerged in the past decade. Mellouli et al. [43] developed a two-dimensional mathematical model that estimated volume changes of approximately 17.77% and 8.16% during hydrogen absorption and desorption, respectively. The model employed separate empirical relations to dynamically track porosity variations during the sorption half-cycles and was validated against their experimental data. Another recent study by Tran et al. [44] investigated the thermo-mechanical behaviour of a hydride bed by incorporating porosity variation using an empirically derived correlation proposed by Matsushita et al. [45]. However, both studies were limited to single-reactor operation and primarily focused on understanding deformation within an isolated bed. In contrast, porosity evolution in coupled reactor configurations is fundamentally different, as it depends on the reacted fraction of both beds. This complex and critical phenomenon remains unaddressed in current literature and warrants immediate investigation, especially for modelling MH-based thermal machines. The predominant scope and inherent limitations of previously reported models along with the distinctive contributions of the present work are summarised in Table 1.

To summarise, there is an urgent need for a comprehensive spatio-temporal mathematical model that addresses shortcomings in existing models by incorporating factors such as volume-change effects, variations in bed permeability due to changes in alloy particle diameter during sorption, pressure hysteresis, sloping plateaux and fluctuations in coolant flow rate. Moreover, this model should be adaptable to various reactor geometries without requiring significant modifications to the governing equations. Such a model would significantly enhance the predictive accuracy and design efficiency of MH systems in real-world

Table 1
Comparison with previously reported models and the present study.

Timeline	Scope and limitation of the studies	References
1980–2000	<ul style="list-style-type: none"> • Most models developed were limited to one-dimensional or two-dimensional formulations. • Studies primarily focused on sensitivity analyses and understanding heat-driven hydrogen transfer phenomena. • Heat transfer was often assumed to occur only in the radial direction. • Models were typically specific to individual reactor configurations. • Coupled heat and mass transfer was simplified, leading to notable deviations from experimental observations. • Boundary conditions were largely theoretical or idealised. • Hydrogen flow within the metal hydride bed was generally not explicitly solved. 	[12–14,17–19]
2000–2010	<ul style="list-style-type: none"> • Three-dimensional formulations were developed and analysed. • Several studies focused on identifying optimal reactor configurations and minimizing reaction time. • Most investigations were limited to single reactor operation, primarily targeting hydrogen storage applications. • None of the studies reported modelling of coupled reactor operation, despite ongoing experimental work on MH-based thermal machines such as refrigerators, heat pumps, and compressors. • Critical phenomena such as hysteresis, sloped pressure plateaus, and alloy bed volume expansion were largely neglected. 	[21,22,24,26,27]
2010–2025	<ul style="list-style-type: none"> • Integrated electrolyser–MH–fuel cell (FC) systems have been reported, though such studies remain limited. • Research efforts continue to emphasise the design and analysis of novel MH reactor configurations. • Models addressing practical thermal machines (e.g., compressors, heat pumps) are scarcely reported. • The few available models are predominantly zeroth-order or one-dimensional and often overlook critical effects such as hysteresis and bed volume expansion. • Most studies do not solve the heat transfer fluid flow explicitly, instead assuming a constant heat transfer coefficient from empirical correlations: An approach that lacks real-world accuracy. • Consequently, alloy suitability for specific thermodynamic applications is often assessed via thermodynamic matching rather than dynamic modelling. 	[7,29,30,33,34,37–39]
Present work	<ul style="list-style-type: none"> • Coupled MH reactor operation has been developed and systematically analysed. • HTF flow is explicitly solved without assuming any constant heat transfer coefficient. • Key MH system phenomena such as volume expansion, hysteresis, and sloping plateau behaviour are incorporated. • A comparative analysis with single-reactor operation models has also been performed. 	

applications.

The distinct contributions of this two-part study, which set it apart from existing literature, are as follows:

- Development of a comprehensive mathematical model to simulate hydrogen transport between two large-scale, interconnected reactors, driven by temperature-induced mass exchange, as happens in real MH machines.

- Incorporation of key factors such as alloy volume change during the exchange process, variable permeability, hysteresis, and HTF flow effects during hydrogen transfer.
- Investigation of spatial variations in thermal gradients and hydrogen transfer rates within the system.
- Examination of the impact of fin design and HTF flow rate on the thermo-hydraulic performance of the MH tanks.

The overall study is structured into two parts. Part 1 (this paper) outlines the comprehensive methodology used to develop the model for studying coupled MH reactors. It elaborates the assumptions and considerations employed to ensure the model closely replicates realistic coupled reactor operations. The model's robustness was validated by comparing its results with experimental data available in the literature. Part 2 explores the model's application in understanding temperature, pressure, and reacted-fraction variations within the coupled reactor beds during operation. Additionally, it highlights the model's advantages over widely studied single-reactor models in the literature.

2. Model formulation

2.1. Model of a coupled MH system

When modelling a single MH bed, hydrogen absorption or desorption at constant pressure simplifies the determination of pressure gradients. However, in a coupled MH bed system, the pressure gradient becomes complex due to multiple influencing parameters. Fig. 1 (a, b) illustrates the hydrogen transfer dynamics between two alloys during coupled MH bed operation. The driving mechanism is the pressure differential, where increasing the desorbing bed temperature and lowering the absorbing bed temperature amplifies the pressure difference ($\Delta P_1 < \Delta P_2 < \Delta P_3$).

Additionally, the hydrogen concentration within each MH particle plays a critical role in determining transfer rates. As shown in Fig. 1 (b), two alloys with different pressure–concentration–temperature (PCT) characteristics exhibit varying rates of pressure reduction. Alloy 1, with a steeper slope, shows a more significant pressure drop during desorption compared to Alloy 2. Although the initial pressure gradient may be favourable (ΔP_{\max}) for hydrogen transfer, the rate of pressure change with respect to hydrogen concentration affects the overall transfer rate. Furthermore, scenarios may arise where the equilibrium pressure of the desorbing bed drops below that of the absorbing bed, halting the transfer process and leaving residual hydrogen in the desorbing bed (ΔC_{res}). Additionally, temperature variations due to the endothermic and exothermic reactions further complicate the behaviour. These factors must be carefully considered when developing mathematical models for coupled MH reactors, which are essential for optimising hydrogen transfer in various engineering applications.

2.2. Geometry of the system and the alloys used

The geometry of the MH reactors used in the current simulation mirrors the design reported by Mohammadshahi et al. [33,34]. This design provides an example of a real-world approach to heat exchange (embedded fin-on-tube) without aiming to achieve optimal performance; in fact the design deliberately anticipates severe temperature gradients as a stringent test of the model. The reactor consists of a cylindrical body with an external diameter of 220 mm, and a central concentric cooling tube with an internal diameter of 20 mm. The heat transfer fluid enters through the inner tube (10 mm inner diameter) and returns through the outer tube after reaching the end of the coolant path. To enhance heat dissipation, 11 transverse copper fins with a diameter of 194 mm are arranged along the coolant tube, as illustrated in Fig. 2. The two end fins, which carry half the heat current of those between, are 1.5 mm thick, while the nine central fins are 3 mm thick. To minimise heat loss and ensure radial heat transfer, the heat-exchange assembly is well insulated at both ends and the tank is covered by an insulating

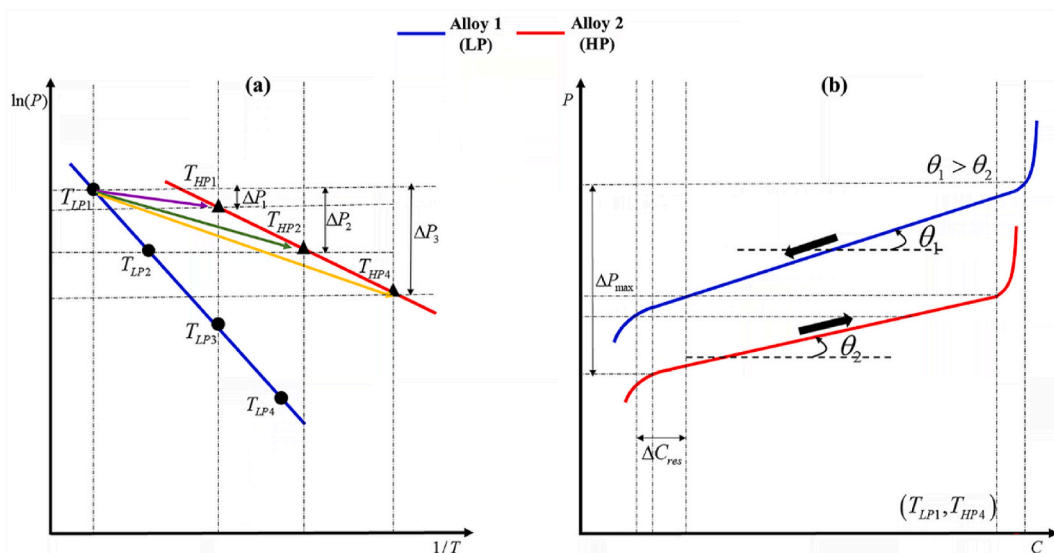


Fig. 1. Schematic representation of operation of coupled reactors in which Alloy 1 (low pressure; LP) desorbs while Alloy 2 (high pressure; HP) absorbs. Panel (a) illustrates the coupling of these two alloy beds, driven solely by temperature ($T_{HP1} > T_{HP2} > T_{HP3} > T_{HP4}$, $T_{LP1} > T_{LP2} > T_{LP3} > T_{LP4}$), and shows the resulting initial pressure difference ($\Delta P_1, \Delta P_2, \Delta P_3$). Panel (b) highlights the complexities encountered when hydrogen mass transfer, linked to changes in H concentration, becomes a function of both bed temperature and concentration. Alloy 1 is maintained at T_{LP1} while alloy 2 is maintained at T_{HP4} during the interstage transfer of hydrogen ($T_{LP1} > T_{HP4}$). The distinct PCT properties of the coupled alloys are demonstrated by considering different slope values $\theta_1 > \theta_2$ ($\theta = \Delta P / \Delta C$), which affect the pressure–concentration relationship during hydrogen transfer.

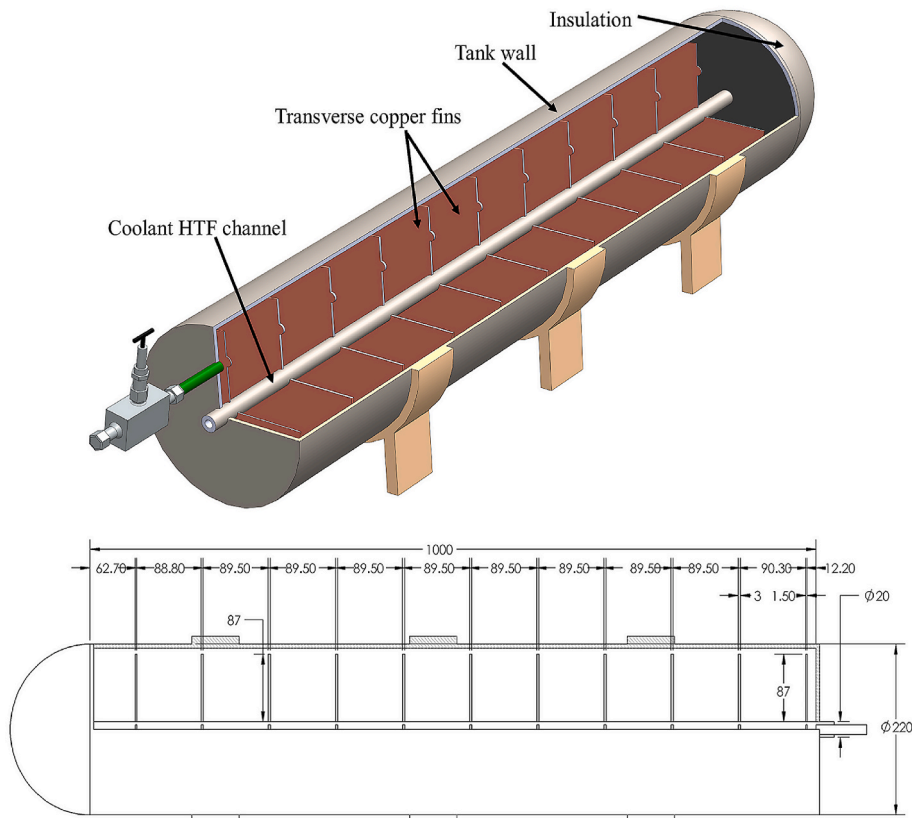


Fig. 2. Detailed geometrical specification of the reactor.

jacket. Given the cylindrical and concentric nature of the reactor, it is logical to study the axisymmetric geometry. This approach can accurately replicate the actual reactor while significantly reducing computation time and cost. The detailed geometry of the MH tank is shown in Fig. 2.

The coupling process occurs between two identical such tanks, labelled Tank A and Tank B, each containing 100 kg of distinct AB₅-type alloys. Tank A is filled with LaNi₅, characterised by low plateau slope and high hysteresis. Tank B contains an equal amount of Mm-Ni-Co-Mn alloy, characterised by a higher plateau slope and lower hysteresis. The

detailed thermo-physical properties are outlined in Table 2. For this study, Tank A was assumed to desorb while Tank B absorbed.

2.3. Mathematical modelling

To simulate the process of hydrogen transport between two MH tanks until chemical, mechanical, and thermal equilibrium is achieved, it is essential to model both mass and heat transfer. Although the chemical reaction is not explicitly simulated, in order to reduce the model's complexity, the reaction enthalpy is included as a heat source term, which will be discussed further. The thermodynamics within the bed during hydrogen transport is addressed using a modified energy equation that assumes local thermal equilibrium. This assumption minimises the number of governing equations required to describe the phenomenon. The model also involves fluid dynamics within the porous bed to simulate the flow of hydrogen from the desorbing porous bed to the absorbing porous bed through an interconnecting tube, driven primarily by the coupled pressure and concentration differences between the beds. Additionally, the model accounts for volume changes during the sorption process. Fig. 3 illustrates the computational domain of the coupled reactor assembly.

To simplify the developed mathematical model, a few assumptions are made, which will be elaborated on below:

- The alloy bed is assumed to possess uniform initial porosity throughout, regardless of location within the bed.
- The alloy bed and hydrogen are assumed to be in a state of local thermal equilibrium.
- Radiative heat transfer is neglected due to the system operating at <100 °C.

2.3.1. Governing equations

2.3.1.1. Conservation of mass. The coupling of two MH tanks necessitates simultaneous mass conservation in both tanks, unlike a single reactor system where a single mass conservation equation suffices. Thus, modelling the hydrogen mass transfer dynamics between the two reactors requires independent yet interrelated mass conservation equations for each tank to accurately capture the transient hydrogen distribution. The specific equations applied within each domain are:

Hydrogen in desorbing MH tank

$$\frac{\partial(\varepsilon\rho_g)}{\partial t} + \nabla \cdot (\rho_g \vec{v}_g) = -\dot{m}_d \quad (2)$$

where ρ_g denotes the density of hydrogen gas and ε denotes the bed porosity, indicating the volume fraction of the bed occupied by

Table 2
Thermophysical data of the alloys used.

Input parameters	LaNi ₅	Mm-Ni-Co-Mn
Empty alloy density (kg.m ⁻³) (ρ_o)	8400	8400
Maximum hydrogen storage capacity (wt%)	1.38	1.4
Initial bed Porosity (ε_i)	0.55	0.55
Reaction enthalpy (J.mol ⁻¹) ($\Delta H_a, \Delta H_d$)	29879	30140
Reaction entropy (J.mol ⁻¹ K ⁻¹) ($\Delta S_a, \Delta S_d$)	112	111.25
Alloy's specific heat capacity (J.kg ⁻¹ K ⁻¹) ($c_{p,mi}$)	500	500
Thermal conductivity (W.m ⁻¹ .K ⁻¹) (k_s)	1.6	1.6
Hysteresis (γ)	0.137	0.12
Reaction constants (s ⁻¹) (C_a, C_d)	9.52	59.187
Activation energy (J/mol) (E_a, E_d)	16445	21170
Slope constant (φ_a, φ_d)	0.038, 0	0.11, 0.07
Initial particle diameter (m) (d_p)	100×10^{-6}	100×10^{-6}
Volume expansion factor (ξ)	1.25	1.25

hydrogen gas. \vec{v}_g denotes the velocity vector for hydrogen gas. \dot{m}_d denotes the mass source term arising from the volumetric desorption of hydrogen from the bed. In summary, the equation characterises the temporal variation in hydrogen density (mass of hydrogen per unit volume within the specified control volume). This change is attributed to the net mass flux, represented by the divergence of the product of density and velocity vector, crossing the control surface, as well as the volumetric mass accumulation within the control volume.

Hydrogen in absorbing MH tank

$$\frac{\partial(\varepsilon\rho_g)}{\partial t} + \nabla \cdot (\rho_g \vec{v}_g) = -\dot{m}_a \quad (3)$$

where the absorbing mass source term is denoted as \dot{m}_a . Inherently, the mass source term should be negative in the absorbing bed due to the migration of hydrogen mass from the hydrogen control volume into the porous bed. Conversely, it must be positive in the desorbing bed. To maintain uniformity in the governing equation, an additional negative sign is incorporated into both source terms. The flow direction is governed by the pressure difference, which is considered in the definition of the mass source term:

Mass source term during desorption:

$$\dot{m}_d = (1 - \varepsilon)C_d \left(\frac{p - P_{eqd}}{P_{eqd}} \right) e^{-\frac{E_d}{RT}} (\rho_{sd} - \rho_{ed}) \quad (4)$$

Mass source term during absorption:

$$\dot{m}_a = (1 - \varepsilon)C_a \log \left(\frac{p}{P_{eqa}} \right) e^{-\frac{E_a}{RT}} (\rho_{sa} - \rho_{sa}) \quad (5)$$

Here, C_d , C_a , E_d and E_a represent respectively the first-order reaction rate constants and activation energies during desorption and absorption. p denotes the pressure of hydrogen flowing in the entire computational domain. The reaction is driven by the pressure difference between the driving pressure and the equilibrium bed pressure, which is governed by temperature and the instantaneous concentration of H in the bed. Thermodynamic drive depends on free-energy difference and is thus expected to be proportional to $\log(p/P_{eq})$. Assuming small pressure difference during desorption, this leads to the commonly employed expressions $\log(p/P_{eqa})$ for absorption and $((p - P_{eqd})/P_{eqd})$ for desorption [17,46–48]. During desorption, the magnitude of p is less than P_{eqd} , making the entire source term negative. Conversely, during absorption, p happens to be more than P_{eqa} , resulting in a positive source term. The transport of hydrogen halts when these differences approach zero. The concentration difference is accounted for by the variation in the density of the porous bed, which results from the addition or removal of hydrogen within the metal alloy. During absorption, the density of the porous bed (ρ_{sa}) increases to approach the saturation density of the absorbing alloy (ρ_{sata}). Conversely, during desorption, the density (ρ_{sd}) decreases to approach the desorbing alloy's density at its empty state (ρ_{ed}). The relationship between the density of the porous bed and the concentration of the solid solution (Ψ) is

$$\Psi = \frac{2(\rho_s - \rho_{ed})M_{alloy}}{\rho_e M_g N_{alloy}} \quad (6)$$

where M_{alloy} and M_g denote the molecular mass of the alloy and of hydrogen gas respectively. N_{alloy} indicates the number of hydrogen atoms that can be absorbed or stored by a single formula unit in a hydride compound, which is notionally 6 for an AB₅ alloy. The instantaneous reacted fraction (X) is evaluated by employing

$$X = \frac{(\rho_s - \rho_{ed})}{(\rho_{sata} - \rho_{ed})} = \frac{\Psi}{\Psi_{max}} \quad (7)$$

Hydrogen in interconnecting tube Hydrogen within the interconnecting domain does not undergo any volumetric mass addition or deduction. Hence, the mass source term is taken as zero:

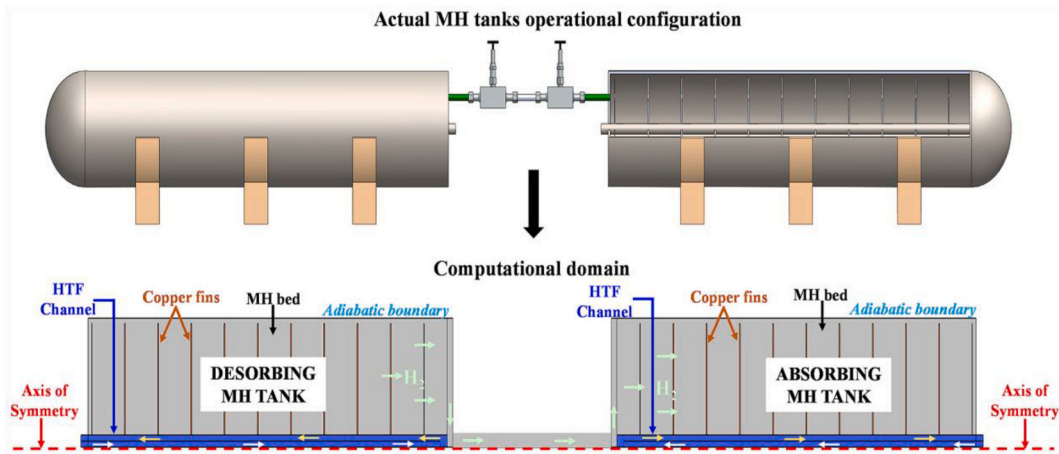


Fig. 3. Detailed computational domain for studying coupled reactors.

$$\frac{\partial(\varepsilon\rho_g)}{\partial t} + \nabla \cdot (\rho_g \vec{v}_g) = 0 \quad (8)$$

Metal alloy in desorbing MH tank

$$(1 - \varepsilon) \frac{\partial(\rho_{sd})}{\partial t} = \dot{m}_d \quad (9)$$

The absence of the divergence term in the mass balance equation for the solid porous matrix simplifies the equation, reducing it to a single degree, first-order ordinary differential equation.

Metal alloy in absorbing MH tank

$$(1 - \varepsilon) \frac{\partial(\rho_{sa})}{\partial t} = \dot{m}_a \quad (10)$$

The mass source term has the opposite sign in the porous alloy bed domain with respect to hydrogen in the corresponding MH bed.

Heat-transfer fluid

$$\frac{\partial(\rho_f)}{\partial t} + \nabla \cdot (\rho_f \vec{v}_f) = 0 \quad (11)$$

Here, ρ_f and \vec{v}_f denote the density and velocity vector respectively of the HTF. No additional mass accumulation takes place during the flow of HTF resulting in a zero-mass source term.

2.3.1.2. Conservation of momentum. The velocity vector and pressure fields are determined by solving the equation for the conservation of momentum. Hydrogen gas migrates through both the porous bed and the interconnecting tube. In contrast, the HTF flows exclusively through the unrestricted domain. Consequently, distinct governing equations are employed for the porous domain and the fluid domain to accurately capture the different transport phenomena.

Hydrogen in desorbing MH tank Momentum conservation for hydrogen gas within the porous domain is modelled by using the Brinkmann equation. While Darcy's Law also addresses momentum conservation for creeping flow ($Re < 1$) through porous media, it represents a simplified form of the more generalised Brinkman equation. Unlike Darcy's Law, the Brinkman formulation allows extension to unrestricted domains by setting the porosity to one, effectively reducing the equation to the classical Navier-Stokes form. This flexibility enabled solutions for the velocity and pressure fields across all regions, including the absorbing and desorbing porous beds as well as the unrestricted interconnecting tube by a single set of dependent variables, which is only feasible with the Brinkman approach.

The first term ($\partial \vec{v}_g / \partial t$) on the left-hand side of the resulting equation (Eqn (12)) encompasses the temporal variations of the velocity vector.

This term represents the local (or temporal) acceleration of the gas, which is the rate of change of the velocity at a point with time. The convective (or advective) term ($\vec{v}_g \cdot \nabla \vec{v}_g$) represents the change in velocity due to the movement of the gas within the velocity field itself. Division by the porosity (ε) accounts for the effective flow area, which is reduced by the presence of the porous matrix. Similarly, the term (ρ_g / ε) normalises the gas density to effectively scale the density based on the available void space. The density of the gas is coupled with the temperature field through the modified ideal gas equation $\rho_g = (pM_g)/(Z(p)RT)$, where $Z(p)$ denotes the compressibility factor of hydrogen, taken to be a function of pressure only in the regime of interest for the present work in the interest of simplicity. The compressibility was modelled as $Z(p[\text{MPa}]) = 0.99725 + 0.007095p + 1.922 \times 10^{-5}p^2$. This expression is accurate to better than 1% in the regime of interest ($T = 250\text{--}400$ K, $p < 5$ MPa) and satisfactory for modelling purposes. Due to the low velocity regime, the convective term can be neglected, simplifying the equation by deleting the second term on the left-hand side.

On the right-hand side, the first term represents the change in pressure per unit distance within the fluid. This term accounts for the driving pressure gradient responsible for the flow of the gas. μ_h denotes the dynamic viscosity of the fluid i.e. hydrogen gas in this case. The Laplacian of the velocity vector ($\nabla \cdot \left[\frac{1}{\varepsilon} \left\{ \mu_h (\nabla \vec{v}_g + (\nabla \vec{v}_g)^T) - \frac{2\mu_h}{3} (\nabla \cdot \vec{v}_g) \right\} \right]$) represents the diffusion of momentum within the fluid accounting for the viscous effects in the fluid flow. The effect of the porous medium is represented by (μ_h / κ) , where κ is the permeability of the porous bed, depicting how easily the fluid can flow through the pores. This term represents the drag force experienced by hydrogen within the porous medium. It is analogous to Darcy's law, which describes the flow through a porous medium driven by a pressure gradient. The term $(\dot{m}_d / \varepsilon^2)$ scales the mass flow rate by the square of the porosity to account for the viscous drag force due to the flow rate through the effective flow area available within the porous medium. The result is

$$\frac{\rho_g}{\varepsilon} \left(\frac{\partial \vec{v}_g}{\partial t} + \vec{v}_g \cdot \nabla \vec{v}_g \right) = -\nabla p + \nabla \cdot \left[\frac{1}{\varepsilon} \left\{ \mu_h (\nabla \vec{v}_g + (\nabla \vec{v}_g)^T) - \frac{2\mu_h}{3} (\nabla \cdot \vec{v}_g) \right\} \right] - \left(\frac{\mu_h}{\kappa} + \frac{\dot{m}_d}{\varepsilon^2} \right) \vec{v}_g \quad (12)$$

Hydrogen in absorbing MH tank

$$\frac{\rho_g}{\varepsilon} \left(\frac{\partial \vec{v}_g}{\partial t} + \vec{v}_g \cdot \nabla \vec{v}_g \right) = -\nabla p + \nabla \cdot \left[\frac{1}{\varepsilon} \left\{ \mu_h \left(\nabla \vec{v}_g + (\nabla \vec{v}_g)^T \right) - \frac{2\mu_h}{3} (\nabla \cdot \vec{v}_g) \right\} \right] - \left(\frac{\mu_h}{\kappa} + \frac{m_a}{\varepsilon^2} \right) \vec{v}_g \quad (13)$$

Hydrogen in interconnecting tube In the unrestricted domain, the terms accounting for the viscous drag due to the porous bed are omitted. With the porosity considered as 1, this simplification results in the standard Navier-Stokes equation:

$$\rho_g \left(\frac{\partial \vec{v}_g}{\partial t} + \vec{v}_g \cdot \nabla \vec{v}_g \right) = -\nabla p + \nabla \cdot \left[\mu_h \left(\nabla \vec{v}_g + (\nabla \vec{v}_g)^T \right) - \frac{2\mu_h}{3} (\nabla \cdot \vec{v}_g) \right] \quad (14)$$

Heat-transfer fluid Similarly, the velocity field of the heat transferring fluid is also simulated by the Navier-Stokes equation. Here, \vec{v}_f, p_f and μ_f denote respectively the velocity vector, pressure and dynamic viscosity of the HTF.

$$\rho_f \left(\frac{\partial \vec{v}_f}{\partial t} + \vec{v}_f \cdot \nabla \vec{v}_f \right) = -\nabla p + \nabla \cdot \left[\mu_f \left(\nabla \vec{v}_f + (\nabla \vec{v}_f)^T \right) - \frac{2\mu_f}{3} (\nabla \cdot \vec{v}_f) \right] \quad (15)$$

2.3.1.3. Conservation of energy. The energy balance equation is solved to investigate the thermodynamic variations within the bed due to hydrogen sorption. Additionally, to examine the energy exchange with the HTF and its potential impact on the rate of hydrogen transfer, the fluid dynamics of the HTF is coupled with the energy equation.

Hydrogen and solid porous alloy bed in MH tank A single governing equation is developed under the assumption of local thermal equilibrium to address the thermodynamics of hydrogen transport within and between the reactors. This equation invokes the bed porosity to simultaneously solve the temperature fields for both hydrogen gas and the porous bed:

$$(\rho c_p)_e \frac{\partial T}{\partial t} + (\rho c_p)_g (\vec{v}_g \cdot \nabla T) = k_e \nabla^2 T - Q_s \quad (16)$$

where $(\rho c_p)_e$ represents the effective heat capacity of the porous bed and hydrogen gas which is determined using Eqn. (17). The second term $(\rho c_p)_g (\vec{v}_g \cdot \nabla T)$ on left hand side of equation represents the transport of thermal energy due to advection.

k_e in Eqn. (16) denotes the effective thermal conductivity (discussed further below). The term $k_e \nabla^2 T$ represents the heat diffusion or dissipation due to temperature gradients within the porous bed. Q_s is the volumetric heat generation term, which accounts for the heat energy released or absorbed to drive the chemical reaction forward or backward. It is evaluated using Eqn. (18), which calculates the product of the volumetric mass flow rate of hydrogen and the enthalpy of formation. The enthalpy of formation is typically negative for this exothermic reaction:

$$(\rho c_p)_e = \varepsilon (\rho c_p)_g + (1 - \varepsilon) (\rho c_p)_s \quad (17)$$

$$Q_s = \dot{m}_{a/d} \left(\frac{\Delta H_{a/d}}{M_g} \right) \quad (18)$$

Transverse copper fins and solid reactor walls

$$\rho_s c_{ps} \frac{\partial T}{\partial t} = k_s \nabla^2 T \quad (19)$$

where ρ_s, c_{ps} and k_s denote respectively the density, heat capacity and thermal conductivity of the solid components of the MH tanks (fins or reactor walls).

Heat-transfer fluid

$$\rho_f c_{pf} \frac{\partial T}{\partial t} + \rho_f c_{pf} (\vec{v}_f \cdot \nabla T) = k_f \nabla^2 T \quad (20)$$

where ρ_f, c_{pf} and k_f denote respectively the density, heat capacity and thermal conductivity of the HTF (assumed to be a 50-50 water-glycol mixture).

2.3.1.4. Effective thermal conductivity. In mathematical modelling, researchers have often assumed constant thermal conductivity throughout the sorption process. However, in reality, the thermal conductivity of the bed varies due to changes in pressure, particle radii, and porosity. The present work employs the Zehner-Bauer-Schlunder (ZBS) model to determine the effective thermal conductivity k_e [16]. The ZBS model incorporates a complex expression that includes multiple parameters, capturing the intricate interplay between different factors affecting thermal conductivity:

$$\frac{k_e}{k_g} = \left(1 - \sqrt{1 - \varepsilon} \right) + \frac{2\sqrt{1 - \varepsilon}}{1 - \frac{k_g}{k_s} B} \left[\frac{\left(1 - \frac{k_g}{k_s} \right) B}{\left(1 - \frac{k_g}{k_s} B \right)^2} \log \left(\frac{k_g}{k_s} B \right) - \frac{B + 1}{2} - \frac{B - 1}{1 - \frac{k_g}{k_s} B} \right] \quad (21)$$

where k_g is the instantaneous thermal conductivity of hydrogen gas. B denotes the deformation factor and is considered as 1 assuming the alloy particle to be spherical. The thermal conductivity of hydrogen gas is evaluated by using Eqn. 22 [49]:

$$k_g = \frac{k_{gref}}{1 + \frac{2b\lambda_m}{d_p}} \quad (22)$$

where k_{gref}, λ_m and b refer to the thermal conductivity of the gas at reference pressure (1 bar), mean free path of the gas and a dimensionless constant (9.87 for H_2), respectively. The mean free path of the gas is assumed to be given by the classical ideal-gas model:

$$\lambda_m = \frac{K_B T}{\sqrt{2} \pi d_{H_2}^2 p} \quad (23)$$

where K_B is the Boltzmann constant and d_{H_2} is the diameter of hydrogen molecule, which is taken as 2.9×10^{-10} m. The equation is coupled with the energy equation for the packed bed to derive the temperature to evaluate mean free path at each time step.

2.3.1.5. Bed porosity. The bed porosity (ε) is defined as the ratio of the void volume (the volume not occupied by solid alloy particles) to the total volume of the reactor, where 0 represents a fully solid bed and 1 represents a completely open space. It is well established that the porosity changes due to the relative expansion and contraction of the solid alloy particles during the absorption and desorption processes, respectively. Wijayanta et al. [50] proposed a robust formula to correlate the instantaneous porosity with the reacted fraction (X), providing a more accurate representation of the dynamic changes in the bed structure:

$$\varepsilon = 1 - (1 - \varepsilon_i) [1 + (\xi - 1)X] \quad (24)$$

where ε_i and ξ denote initial bed porosity (assumed to be 0.5 in the present case) and expansion coefficient (1.25 for AB₅ type alloy), respectively [4]. The alloy bed consists of irregularly shaped particles that are computationally challenging to model. Therefore, the particles are approximated as regular spheres with a defined initial diameter, which changes during the sorption process based on the alloy's expansion coefficient. The solver dynamically accounts for this variation, partitioning the computational domain into separate regions corresponding to the varying occupied volume within a constant bed volume, as illustrated in Fig. 4. Overall, the volume change of the alloy bed during sorption is accommodated through variations in porosity, while the buffer space volume remains constant throughout the process. This approach reduces the complexity of the heterogeneous domain, treating it as two homogeneous subdomains while capturing the inherent heterogeneities through empirical relations coupled with variables like temperature, alloy density, hydrogen velocity, and mass of absorbed hydrogen.

2.3.1.6. Bed permeability. The permeability (κ) of the packed bed is dependent on the particle size and bed porosity. It is determined by Kozeny-Carman's equation:

$$\kappa = \frac{d_p^2 \varepsilon^3}{180(1 - \varepsilon)^2} \quad (25)$$

The particles are assumed to be spherical with a diameter d_p , which is assumed to expand or contract according to

$$d_p = d_{p_i} [1 + (\xi - 1)X]^{1/3} \quad (26)$$

2.3.1.7. Equilibrium pressure. The equilibrium pressure within the MH bed during the sorption process is calculated using a modified van't Hoff equation that incorporates pressure hysteresis and plateau slope to provide a more accurate representation of the equilibrium conditions [25]:

$$\log\left(\frac{P_{eq}(X)}{P_o}\right) = -\frac{|\Delta H|}{RT} + \frac{\Delta S}{R} + (\varphi_s \pm \varphi_o) \tan[\pi \times (X - 0.5)] \pm \frac{\gamma}{2} \quad (27)$$

In this context, the positive sign is used during the absorption process, and the negative sign is used during desorption. The fitted parameters φ_s and φ_o account for plateau slope while γ incorporates the effect of hysteresis.

2.4. Initial value and boundary conditions

The governing equations are solved by invoking the initial values and boundary conditions listed in Table 3.

2.5. Numerical procedure and implementation in software

The 2-D axisymmetric numerical model was developed using COMSOL Multiphysics 6.1. The governing equations were applied to their respective domains using built-in physics interfaces and specific user-defined functions. Mass and momentum conservation for hydrogen gas and the HTF were simulated by incorporating the *Brinkman Equation* and *Laminar Flow* physics modules, respectively. Mass conservation for the solid alloy bed was addressed through an independent ordinary differential equation. Energy conservation across all domains was modelled using the *Heat Transfer in Fluids* physics module. Additionally, the *Non-Isothermal Flow* Multiphysics interface couples laminar flow and heat transfer within the HTF domain. The model employs a segregated approach under a time-dependent solver to manage the numerical integration of partial differential equations (PDEs) over time. Given the potential for asymmetrical matrices, the PARDISO linear solver was used, with a relative tolerance set to 0.0005.

3. Validation of mathematical model with reported literature

The developed model was rigorously validated by comparing its predictions with experimental datasets reported by Ni and Liu [51], who explored a MH-based refrigeration system comprising two high-pressure beds containing LaNi_{4.6}Mn_{0.26}Al_{0.13} and two-low pressure beds containing La_{0.6}Y_{10.4}Ni_{4.8}Mn_{0.2}. The present model was configured to replicate the identical geometry (50 mm outer diameter and 500 mm length) and alloys used in the experimental studies. Critical properties, such as hysteresis and plateau slope, are derived from the Pressure-Composition-Temperature (PCT) data of the alloys. Fig. 5 presents the predicted temperature evolution when the high-pressure bed was initially heated to 403 K and 423 K. The comparison reveals a maximum discrepancy of < 3% between the predicted and the experimental temperatures. This minor discrepancy is likely due to inherent bed heterogeneities and their temperature-dependent variations, which are treated as constants in the current mathematical framework. This validation underscores the model's robustness while highlighting areas for potential refinement to account for complex physical phenomena.

4. Summary and conclusions

A two-dimensional axisymmetric model was developed, using the finite-element method in COMSOL Multiphysics, to simulate hydrogen transport between two cylindrical MH reactors, each equipped with transverse copper fins and a central coolant flow channel. This configuration was chosen to generate strong temperature gradients, prediction of which would constitute a stringent test of the model in experiments with real tanks built to a similar design. The model was tested against an experimental study reported in the literature. The temporal temperature variation predicted by the model was within 3% of the experimental values, underscoring the robustness and reliability of the model for

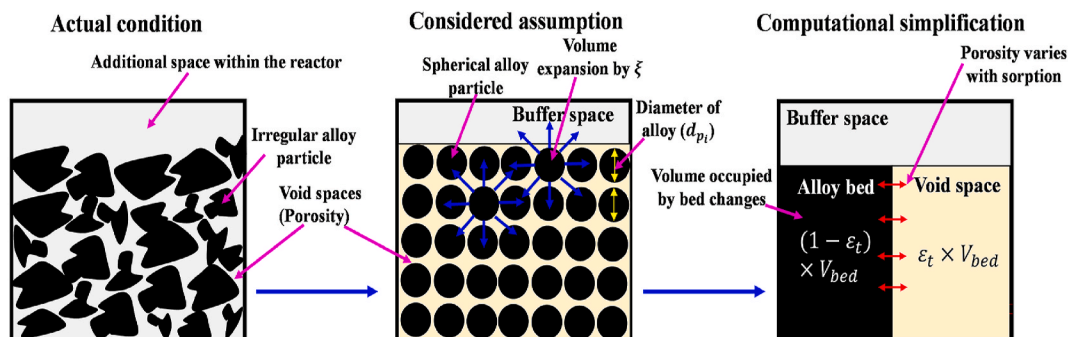


Fig. 4. Computational simplification to consider the volume change effects.

Table 3
Initial value and boundary conditions.

Equation no.	Order of equation	Initial value	Boundary condition
Mass conservation			
(2)	First order in time and second order in space	1) The initial density of the gas desorbing from desorbing MH tank is evaluated at initial desorbing bed temperature and pressure. $\rho_g(r, z, 0) = \frac{p_i M_g}{Z(p) R T_i}$	1) Flow continuity on the walls connecting with interconnecting tube and hydrogen filter. 2) No slip condition at the reactor and fin surface. $\vec{v}_{\mathcal{G}_{\text{solid surface}}} = 0$
(3)	First order in time and second order in space	1) The initial density of the gas being absorbed by the MH tank is evaluated at initial absorbing bed temperature and pressure. $\rho_g(r, z, 0) = \frac{p_i M_g}{Z(p) R T_i}$	1) Flow continuity on the walls connecting with interconnecting tube and hydrogen filter. 2) No slip condition at the reactor and fin surface. $\vec{v}_{\mathcal{G}_{\text{solid surface}}} = 0$
(8)	First order in time and second order in space	1) The initial density of the gas is evaluated at P_{gi} and T_{gi} . $\rho_g(r, z, 0) = \frac{P_{gi} M_g}{Z(p) R T_{gi}}$ $T_{gi} = \frac{m_d T_{di} + m_a T_{ai}}{m_d + m_a}$ $m_d = \frac{P_{eqdi} V_{MHT} M_g}{Z(p) R T_{di}}$ $m_a = \frac{P_{eqai} V_{MHT} M_g}{Z(p) R T_{ai}}$ $P_{gi} = \frac{(m_d + m_a) Z(p) R T_{gi}}{M_g V_{\text{tube}}}$	1) Flow continuity on the walls connecting with both the MH tank. 2) No slip condition at tube surface. $\vec{v}_{\mathcal{G}_{\text{solid surface}}} = 0$
(9)	First order in time	1) The initial bed density is determined at $\Psi = 0.95$. $\rho_{sd}(r, z, 0) = \rho_{sdi}$	Not required
(10)	First order in time	1) The initial bed density is determined at $\Psi = 0.05$. $\rho_{sai}(r, z, 0) = \rho_{sai}$	Not required
(11)	First order in time and second order in space	1) Density is fixed (incompressible fluid)	1) No slip condition at the coolant tube inner surface
Momentum conservation			
(12)	First order in time and second order in space	1) Bed pressure is initialised with P_{gi} for 0.05 s and then stepped up to the initial equilibrium pressure P_{eqdi} using step function $S(t)$. $p_i = P_{gi} - (S(t) \times (P_{gi} - P_{eqdi}))$ 2) Initial velocity is zero. $\vec{v}_{gi} = 0$	1) Flow continuity on the walls connecting interconnecting tube. 2) No slip condition at tube surface. $\vec{v}_{\mathcal{G}_{\text{solid surface}}} = 0$ 3) Symmetry boundary condition.
(13)	First order in time and second order in space	1) Bed pressure is initialised with P_{gi} for 0.05 s and then stepped up to the initial equilibrium pressure P_{eqai} using step function $S(t)$. $p_i = P_{gi} - (S(t) \times (P_{gi} - P_{eqai}))$ 2) Initial velocity is zero. $\vec{v}_{gi} = 0$	1) Flow continuity on the walls connecting interconnecting tube. 2) No slip condition at tube surface. $\vec{v}_{\mathcal{G}_{\text{solid surface}}} = 0$ 3) Symmetry boundary condition.
(14)	First order in time and second order in space	1) Bed pressure is initialised with P_{gi} . 2) Initial velocity is zero. $\vec{v}_{gi} = 0$	1) Flow continuity on the walls connecting both the MH tank. 2) No slip condition at tube surface. $\vec{v}_{\mathcal{G}_{\text{solid surface}}} = 0$ 3) Symmetry boundary condition.
(15)	First order in time and second order in space	1) Initial HTF velocity and pressure are zero. $\vec{v}_{fi} = 0$ $p_{fi} = 0$	1) Inlet mass flux $\left(\frac{\dot{m}_f}{A_{\text{inlet}}}\right)$ is invoked at HTF inlet. $\vec{v}_{\text{inlet}} = \frac{\dot{m}_f}{A_{\text{inlet}}}$ 2) Outlet condition at HTF tube outlet. 3) Symmetry boundary condition.
Energy conservation			
(16)	First order in time and second order in space	1) Bed temperature is initialised to the corresponding absorption and desorption temperature. $T(r, z, 0) = T_{ai/di}$	1) Heat flux continuity. $-k_e \nabla T _{MH} = -k_{HEX} \nabla T _{HEX}$ 2) Symmetry boundary condition.
(19)	First order in time and second order in space	1) Fin and reactor temperature are initialised to the corresponding bed temperature. $T(r, z, 0) = T_{ai/di}$	1) Heat flux continuity. $-k_e \nabla T _{MH} = -k_{HEX} \nabla T _{HEX}$ 2) Adiabatic condition on the outer reactor walls. $\frac{\partial T}{\partial n} = 0$
(20)	First order in time and second order in space	1) HTF temperature is initialised to the corresponding absorption and desorption bed temperature. $T(r, z, 0) = T_{ai/di}$	1) Inlet temperature is invoked at HTF inlet. $T_{\text{inlet}} = T_{ai/di}$ 2) Outlet condition at HTF tube outlet. 3) Symmetry boundary condition.

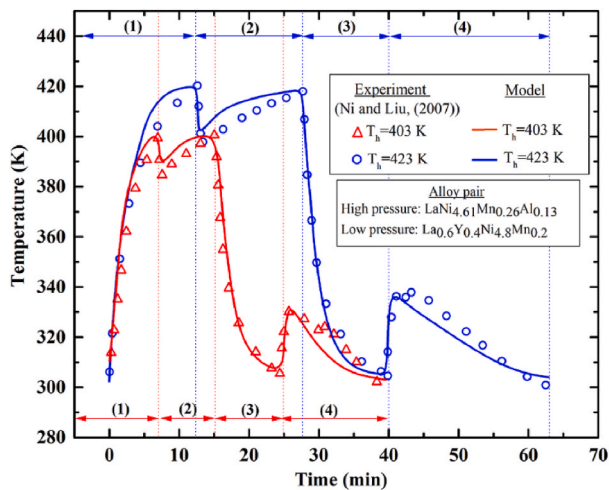


Fig. 5. Validation of the developed model with the experimental datasets of Ni and Liu [51]. The temperature in the high-pressure bed ($\text{LaNi}_{4.6}\text{Mn}_{0.26}\text{Al}_{0.13}$) was recorded during a sequence in which it was heated to T_h (403 K and 423 K) (1), followed by dehydrogenating (2) after which the bed was cooled to T_l (3) before absorbing hydrogen (4) from the low-pressure bed ($\text{La}_{0.6}\text{Y}_{0.4}\text{Ni}_{4.8}\text{Mn}_{0.2}$).

simulating the hydrogen transport dynamics between metal hydride reactors. The following paper presents the results of a detailed study of coupled reactor operation employing the developed model.

CRedit authorship contribution statement

Abhishek Parida: Writing – original draft, Validation, Software, Formal analysis, Data curation, Conceptualization. **Evan MacA. Gray:** Writing – review & editing, Supervision, Project administration, Funding acquisition, Conceptualization. **P. Muthukumar:** Supervision. **Amaresh Dalal:** Supervision.

Declaration of competing interest

The authors declare that they have no known competing financial interests or personal relationships that could have appeared to influence the work reported in this paper.

Acknowledgement

AP acknowledges the receipt of a Griffith University Postgraduate Research Scholarship for carrying out the work.

References

- [1] Fukai Y. The metal-hydrogen system. second ed. Berlin, Heidelberg: Springer; 2005. <https://doi.org/10.1007/3-540-28883-X>. vol. 1.
- [2] Mohammadshahi SS, Gray EMacA, Webb CJ. A review of mathematical modelling of metal-hydride systems for hydrogen storage applications. *Int J Hydrogen Energy* 2016;41:3470–84. <https://doi.org/10.1016/j.ijhydene.2015.12.079>.
- [3] Lototskyy MV, Tarasov BP, Yartys VA. Gas-phase applications of metal hydrides. *J Energy Storage* 2023;72:108165. <https://doi.org/10.1016/j.est.2023.108165>.
- [4] Lototskyy MV, Yartys VA, Pollet BG, Bowman RC. Metal hydride hydrogen compressors: a review. *Int J Hydrogen Energy* 2014;39:5818–51. <https://doi.org/10.1016/j.ijhydene.2014.01.158>.
- [5] Muthukumar P, Kumar A, Raju NN, Malleswararao K, Rahman MM. A critical review on design aspects and developmental status of metal hydride based thermal machines. *Int J Hydrogen Energy* 2018;43:17753–79. <https://doi.org/10.1016/j.ijhydene.2018.07.157>.
- [6] Dantzer P, Orgaz E. Thermodynamics of hydride chemical heat pump-II. How to select a pair of alloys. *Int J Hydrogen Energy* 1986;11:797–806. [https://doi.org/10.1016/0360-3199\(86\)90176-X](https://doi.org/10.1016/0360-3199(86)90176-X).
- [7] EmacA Gray. Alloy selection for multistage metal-hydride hydrogen compressors: a thermodynamic model. *Int J Hydrogen Energy* 2021;46:15702–15. <https://doi.org/10.1016/j.ijhydene.2021.02.025>.
- [8] Cousins A, Zohra FT, Gray EMacA, Webb CJ, Kochanek M, Edwards S, et al. Alloy selection for dual stage metal-hydride hydrogen compressor: using a thermodynamic model to identify metal-hydride pairs. *Int J Hydrogen Energy* 2023;48:28453–9. <https://doi.org/10.1016/j.ijhydene.2023.03.365>.
- [9] Wiswall RH, Reilly JJ. Method of storing hydrogen. 1970.
- [10] Van Mal HH, Buschow KHJ, Miedema AR. Hydrogen absorption in LaNi_5 and related compounds: experimental observations and their explanation. *J Less-Common Met* 1974;35:65–76. [https://doi.org/10.1016/0022-5088\(74\)90146-5](https://doi.org/10.1016/0022-5088(74)90146-5).
- [11] Diaz H, Percheron-Guégan A, Achard JC, Chatillon C, Mathieu JC. Thermodynamic and structural properties of $\text{LaNi}_5\text{-yAl}_y$ compounds and their related hydrides. *Int J Hydrogen Energy* 1979;4:445–54. [https://doi.org/10.1016/0360-3199\(79\)90104-6](https://doi.org/10.1016/0360-3199(79)90104-6).
- [12] El Oesry IA. Theory of the computer code RET 1 for the calculation of space-time dependent temperature and composition properties of metal hydride hydrogen storage beds. *Int J Hydrogen Energy* 1983;8:191–8. [https://doi.org/10.1016/0360-3199\(83\)90064-2](https://doi.org/10.1016/0360-3199(83)90064-2).
- [13] Lucas GG, Richards WL. Mathematical modelling of hydrogen storage systems. *Int J Hydrogen Energy* 1984;9:225–31. [https://doi.org/10.1016/0360-3199\(84\)90123-X](https://doi.org/10.1016/0360-3199(84)90123-X).
- [14] Sun D-W, Deng S-J. Study of the heat and mass transfer characteristics of metal hydride beds: a two-dimensional model. *J Less-Common Met* 1989;155:271–9.
- [15] Goodell PD, Rudman PS. Hydriding and dehydriding rates of the $\text{LaNi}_5\text{-H}$ system. *J Less-Common Met* 1983;89:117–25. [https://doi.org/10.1016/0022-5088\(83\)90255-2](https://doi.org/10.1016/0022-5088(83)90255-2).
- [16] Pons M, Dantzer P. Effective thermal conductivity in hydride packed beds. Study of basic mechanisms with help of the bauer and schlünder model. *J Less-Common Met* 1991;172–174:1147–56. [https://doi.org/10.1016/S0022-5088\(06\)80022-6](https://doi.org/10.1016/S0022-5088(06)80022-6).
- [17] Jemni A, Nasrallah S Ben. Study of two-dimensional heat and mass transfer during desorption in a metal-hydrogen reactor. *Int J Hydrogen Energy* 1995;20:881–91. [https://doi.org/10.1016/0360-3199\(94\)00115-G](https://doi.org/10.1016/0360-3199(94)00115-G).
- [18] Ben Nasrallah S, Jemni A. Heat and mass transfer models in metal-hydrogen reactor. *Int J Hydrogen Energy* 1997;22:67–76. [https://doi.org/10.1016/s0360-3199\(96\)00039-0](https://doi.org/10.1016/s0360-3199(96)00039-0).
- [19] Jemni A, Nasrallah S Ben, Lamoumi J. Experimental and theoretical study of a metal-hydrogen reactor. *Int J Hydrogen Energy* 1999;24:631–44. [https://doi.org/10.1016/S0360-3199\(98\)00117-7](https://doi.org/10.1016/S0360-3199(98)00117-7).
- [20] Mellouli S, Askri F, Dhaou H, Jemni A, Ben Nasrallah S. Numerical simulation of heat and mass transfer in metal hydride hydrogen storage tanks for fuel cell vehicles. *Int J Hydrogen Energy* 2010;35:1693–705. <https://doi.org/10.1016/j.ijhydene.2009.12.052>.
- [21] Mellouli S, Askri F, Dhaou H, Jemni A, Ben Nasrallah S. Numerical study of heat exchanger effects on charge/discharge times of metal-hydrogen storage vessel. *Int J Hydrogen Energy* 2009;34:3005–17. <https://doi.org/10.1016/j.ijhydene.2008.12.099>.
- [22] Muthukumar P, Madhavakrishna U, Dewan A. Parametric studies on a metal hydride based hydrogen storage device. *Int J Hydrogen Energy* 2007;32:4988–97. <https://doi.org/10.1016/j.ijhydene.2007.08.010>.
- [23] Muthukumar P, Singhal A, Bansal GK. Thermal modeling and performance analysis of industrial-scale metal hydride based hydrogen storage container. *Int J Hydrogen Energy* 2012;37:14351–64. <https://doi.org/10.1016/j.ijhydene.2012.07.010>.
- [24] Muthukumar P, Ramana SV. Numerical simulation of coupled heat and mass transfer in metal hydride-based hydrogen storage reactor. *J Alloys Compd* 2009;472:466–72. <https://doi.org/10.1016/j.jallcom.2008.04.088>.
- [25] Nishizaki T, Miyamoto K, Yoshida K. Coefficients of performance of hydride heat pumps. *J Less-Common Met* 1983;89:559–66. [https://doi.org/10.1016/0022-5088\(83\)90372-7](https://doi.org/10.1016/0022-5088(83)90372-7).
- [26] Hardy BJ, Anton DL. Hierarchical methodology for modeling hydrogen storage systems. Part II: detailed models. *Int J Hydrogen Energy* 2009;34:2992–3004. <https://doi.org/10.1016/j.ijhydene.2008.12.056>.
- [27] Hardy BJ, Anton DL. Hierarchical methodology for modeling hydrogen storage systems. Part I: scoping models. *Int J Hydrogen Energy* 2009;34:2269–77. <https://doi.org/10.1016/j.ijhydene.2008.12.070>.
- [28] Bhourri M, Goyette J, Hardy BJ, Anton DL. Sensitivity study of alanate hydride storage system. *Int J Hydrogen Energy* 2011;36:621–33. <https://doi.org/10.1016/j.ijhydene.2010.10.009>.
- [29] Krishna KV, Pandey V, Maiya MP. Bio-inspired leaf-vein type fins for performance enhancement of metal hydride reactors. *Int J Hydrogen Energy* 2022;47:23694–709. <https://doi.org/10.1016/j.ijhydene.2022.05.163>.
- [30] Nyamsi SN, Yang F, Zhang Z. An optimization study on the finned tube heat exchanger used in hydride hydrogen storage system - analytical method and numerical simulation. *Int J Hydrogen Energy* 2012;37:16078–92. <https://doi.org/10.1016/j.ijhydene.2012.08.074>.
- [31] Bao Z, Wu Z, Nyamsi SN, Yang F, Zhang Z. Three-dimensional modeling and sensitivity analysis of multi-tubular metal hydride reactors. *Appl Therm Eng* 2013;52:97–108. <https://doi.org/10.1016/j.applthermaleng.2012.11.023>.
- [32] Raju M, Kumar S. System simulation modeling and heat transfer in sodium alanate based hydrogen storage systems. *Int J Hydrogen Energy* 2011;36:1578–91. <https://doi.org/10.1016/j.ijhydene.2010.10.100>.
- [33] Mohammadshahi SS, Gould T, Gray EMacA, Webb CJ. An improved model for metal-hydrogen storage tanks - part 1: model development. *Int J Hydrogen Energy* 2016;41:3537–50. <https://doi.org/10.1016/j.ijhydene.2015.12.050>.
- [34] Mohammadshahi SS, Gould T, Gray EMacA, Webb CJ. An improved model for metal-hydrogen storage tanks - part 2: model results. *Int J Hydrogen Energy* 2016;41:3919–27. <https://doi.org/10.1016/j.ijhydene.2015.12.051>.
- [35] Parida A, Kumar A, Muthukumar P, Dalal A. Experimental and numerical investigations on synergistic coupling of metal hydride hydrogen storage systems with low-temperature proton exchange membrane fuel-cell. *Therm Sci Eng Prog* 2024;51:102620. <https://doi.org/10.1016/j.tsep.2024.102620>.

- [36] Arslan B, Ilbas M, Celik S. Experimental analysis of hydrogen storage performance of a LaNi₅-H₂ reactor with phase change materials. *Int J Hydrogen Energy* 2023;48:6010–22. <https://doi.org/10.1016/j.ijhydene.2022.11.083>.
- [37] d'Entremont A, Corgnale C, Sulic M, Hardy B, Zidan R, Motyka T. Modeling of a thermal energy storage system based on coupled metal hydrides (magnesium iron–sodium alanate) for concentrating solar power plants. *Int J Hydrogen Energy* 2017;42:22518–29. <https://doi.org/10.1016/j.ijhydene.2017.04.231>.
- [38] Malleswararao K, N A, Srinivasa Murthy S, Dutta P. Performance prediction of a coupled metal hydride based thermal energy storage system. *Int J Hydrogen Energy* 2020;45:16239–53. <https://doi.org/10.1016/j.ijhydene.2020.03.251>.
- [39] Minko KB, Bocharnikov MS, Yanenko YB, Lototsky MV, Kolesnikov A, Tarasov BP. Numerical and experimental study of heat-and-mass transfer processes in two-stage metal hydride hydrogen compressor. *Int J Hydrogen Energy* 2018;43:21874–85. <https://doi.org/10.1016/j.ijhydene.2018.09.211>.
- [40] Gkanas EI, Stamatakis E, Christodoulou CN, Tzamalís G, Karagiorgis G, Chronos A, et al. Study on the operation and energy demand of dual-stage metal hydride hydrogen compressors under effective thermal management. *Int J Hydrogen Energy* 2021;46:29272–87. <https://doi.org/10.1016/j.ijhydene.2021.02.062>.
- [41] Askri F, Mellouli S, Alqahtani T, Algarni S, Alshammari BM, Kolsi L. Performance improvement of metal hydride hydrogen compressors using electromagnetic induction heating. *Alex Eng J* 2024;98:103–13. <https://doi.org/10.1016/j.aej.2024.04.047>.
- [42] Bhogilla SS. Numerical simulation of metal hydride based thermal energy storage system for concentrating solar power plants. *Renew Energy* 2021;172:1013–20. <https://doi.org/10.1016/j.renene.2021.03.109>.
- [43] Mellouli S, Askri F, Dhaou H, Jemni A, Ben Nasrallah S. A study of the thermal behavior of a deformable metal-hydride bed. *Int J Hydrogen Energy* 2016;41:1711–24. <https://doi.org/10.1016/j.ijhydene.2015.10.058>.
- [44] Tran DP, La MP, Lototsky MV. Stress analysis of cyclic sorption-desorption in metal hydride vessels. *J Energy Storage* 2024;98:112868. <https://doi.org/10.1016/j.est.2024.112868>.
- [45] Matsushita M, Monde M, Mitsutake Y. Experimental formula for estimating porosity in a metal hydride packed bed. *Int J Hydrogen Energy* 2013;38:7056–64. <https://doi.org/10.1016/j.ijhydene.2013.04.005>.
- [46] Mellouli S, Askri F, Alqahtani T, Algarni S, Mohamed Zribi S. Numerical assessment of a thermal energy storage system based on a metal hydride reactor and a mechanical hydrogen compressor. *Appl Therm Eng* 2024;243:122670. <https://doi.org/10.1016/j.applthermaleng.2024.122670>.
- [47] Jemni A, Nasrallah S Ben. Study of two-dimensional heat and mass transfer during absorption in a metal-hydrogen reactor. *Int J Hydrogen Energy* 1995;20:43–52. [https://doi.org/10.1016/0360-3199\(93\)E0007-8](https://doi.org/10.1016/0360-3199(93)E0007-8).
- [48] Chang H, Tao YB, Wang WY. Numerical study on storage performance of metal hydride reactors with multiple spiral fins. *Int J Hydrogen Energy* 2023;48:35170–84. <https://doi.org/10.1016/j.ijhydene.2023.05.248>.
- [49] Lin X, Zhu Q, Leng H, Yang H, Lyu T, Li Q. Numerical analysis of the effects of particle radius and porosity on hydrogen absorption performances in metal hydride tank. *Appl Energy* 2019;250:1065–72. <https://doi.org/10.1016/j.apenergy.2019.04.181>.
- [50] Wijayanta AT, Nakaso K, Aoki T, Kitazato Y, Fukai J. Effect of pressure, composition and temperature characteristics on thermal response and overall reaction rates in a metal hydride tank. *Int J Hydrogen Energy* 2011;36:3529–36. <https://doi.org/10.1016/j.ijhydene.2010.12.047>.
- [51] Ni J, Liu H. Experimental research on refrigeration characteristics of a metal hydride heat pump in auto air-conditioning. *Int J Hydrogen Energy* 2007;32:2567–72. <https://doi.org/10.1016/j.ijhydene.2006.09.038>.